Electric Current Density Imaging of Mice Tumors

Igor Serša, Katarina Beravs, Nick J. F. Dodd, Sha Zhao, Damijan Miklavčič, Franci Demsar

The use of electric current density imaging (CDI) to map spatial distribution of electric currents through tumors is presented. Specifically, a method previously tested on phantoms was implemented *in vivo* and *in vitro* for mapping electric current pulses of the same order of magnitude ($j \cong 2500$ A/m^2) as in electrochemotherapy through T50/80 mammary carcinomas, B-16 melanomas and SA-1 sarcomas. A technically simplified method of electric current density imaging is discussed as well. Three geometries of electrodes (flat-flat, point-point, point-flat) indicate altered electric current distribution for the same tumor. This indicates that the method can be used for monitoring the effects of electrochemotherapy as a function of electrode geometry.

Key words: magnetic resonance imaging (MRI); current density imaging (CDI); electrochemotherapy (ECT); tumors.

INTRODUCTION

Electrotherapy is a relatively well established and efficient method of tumor treatment (1) in which most commonly one electrode—a needle—is implanted into the tumor, and the other—a needle or a larger plate—is placed somewhere far from the tumor (2-5). Some authors propose insertion of both electrodes into the tumor (2, 6, 7). Electrodes can be also placed on the surface (8) or besides the tumor to the opposite sides, so that the tumor is located between them and thus the current flows through it (9). Literature data suggest possible antitumor mechanisms such as: changing the bioelectric potential of the tumor (10), deposition of metal ions (11-13) and electrochemical reactions in the vicinity of the electrodes, the results of which can be cytotoxic products leading to the changes of pH values within the tissues (9, 14-16). Also, electric field pulses used for cell manipulation can cause irreversible cell damage by free radical mediated processes such as lipid peroxidation of the cell membrane and/or lipid degradation or fragmentation that results in cytolysis (17). Most of these effects depend on electric field intensity.

Recently a novel method of treating cancer by a combination of an electric field with chemotherapeutic agents was introduced (18). The technique is known as electrochemotherapy (ECT). ECT is designed to overcome one of the problems of chemotherapy—that is, cytotoxicity of antitumor agents such as bleomycin is limited by the rate at which the drug enters the cell. It has been demonstrated that uptake of various drugs by the tumor cells can be increased markedly by ECT (19-22). Electropermeabilization of the tumor cell membranes by a local application of short, intense electric pulses, enables cell drug uptake, thus potentiating cytostatic effect and reducing the dose of drug required and thereby minimizes undesired side effects. Moreover, ECT followed by injection of a low dose of interleukin-2 (IL-2) or IL-2 secreting cells has shown better results than ECT alone (21, 22). There appears to be a systemic effect and a strong indication that an immune response may be elicited by this method of treatment. Results suggest that ECT combined with such cellular immunotherapy might be a useful approach for the treatment of metastasing cancers (23). However, the efficiency of electrochemotherapy is highly dependent on the magnitude and spatial distribution of electric currents flowing through the tumor and its surrounding tissue.

Due to inhomogeneous nature of tissues conductivity, direct measurements of spatial distribution of electric currents are highly desirable. Current density imaging (CDI) with MRI provides a tool to examine them (24).

CDI is a relatively new MRI technique that has been experimentally demonstrated on phantoms (24) and biological tissues (25-29). Theoretical consideration of sensitivity and resolution on a model system have shown that by proper optimization of the procedure, similar signal-to-noise ratios (SNR) to those obtained in conventional MRI can be achieved in biologically relevant experiments (24, 25). In CDI, short pulses of electric current are passed through the sample, causing a transient shift in the static magnetic field. The two DC pulses are synchronized with the conventional spin warp imaging sequence (24, 25) and applied symmetrically about the π pulse, with the first between the RF $\pi/2$ and π pulses, and the second between the RF π pulse and signal acquisition. The electric pulses have the same magnitude and duration, but opposite polarity. Since the currents are pulsed, this produces a phase shift (ϕ) in the proton image, proportional to the magnetic field change and the duration of the pulse. Imaging phase shift in nuclear precession provides a map of magnetic field change seen on the real component of the signal (S) as stripes superimposed on the image:

$$S = S_0 \sin\varphi \qquad [1]$$

where S_0 indicates conventional magnitude image. Phase measurements only reflect the component of the induced field along the direction of the main magnetic field. To obtain a complete map of current density (CD), the sample should be rotated and images obtained in three orthogonal directions, while two directions are necessary to calculate current density in a plane. For example, calculating current density (j_z) in the xy plane requires

MRM 37:404–409 (1997)

From the Jožef Stefan Institute, University of Ljubljana, Ljubljana, Slovenia (I. S., K. B., D. M., F. D.); and Paterson Institute for Cancer Research (S. Z.), and Manchester University Medical School (S. Z.), Manchester, United Kingdom.

Address correspondence to: Franci Demsar "Josef Stefan" Institute, University of Ljubljana, Jamova 100, 61111 Ljubljana, Slovenia.

Received February 7, 1996; revised August 5, 1996; accepted August 19, 1996.

This research was supported, in part, by the Cancer Research Campaign and British Council.

0740-3194/97 $3.00

that $B_{\text{current-x}}$ and $B_{\text{current-y}}$ must be determined from images in the xy plane in two sample orientations 90° apart about the z axis. Current density (j_z) is calculated on a pixel-by-pixel basis using Ampere's law:

$$j_z = 1/\mu_0(\partial B_{\text{current-y}}/\partial x - \partial B_{\text{current-x}}/\partial y) \qquad [2]$$

From the complex NMR signal, phase image (in the module of 2 π) was obtained for two experiments: first in which $B_{\text{current-x}}$ field was measured (B_0 was parallel to $x$axis of the sample) and second in which $B_{\text{current-y}}$ field was measured (B_0 was parallel to y axis of the sample). The current density image was calculated as a difference between gradient in the x direction of the B_y phase image and gradient in the y direction of the B_x phase image.

In this study we present the use of CDI to map spatial distribution of electric currents through tumors *in vivo* and *in vitro*. We also emphasize the importance of the geometry of the electric field lines defined by electrodes for permeabilizing a whole tissue, i.e., a tumor (30), which can be studied by CDI. In the case of some tumors, this method can be technically simplified by numerical simulation.

MATERIALS AND METHODS

In Vivo Measurements

Experiments on CDI of tumors were conducted on four T50/80 mammary carcinomas grown subcutaneously on the flanks of nude immunosuppressed mice. Tumors were approximately 1 cm in diameter. During the experiments, mice were maintained under inhalation anesthesia and were placed in a Perspex tube with a longitudinal slot, in such a way that the subcutaneously implanted tumor was positioned outside the tube. One electrode consisted of short copper strips on either side of the slot, connected by a larger strip around the tube to make contact with the base of the tumor. The second electrode was a thick gold wire, positioned vertically, to made contact with the top of the tumor (Fig. 1a).

In Vitro Measurements

Four SA-1 sarcomas grown subcutaneously on the flanks of male A/J mice and two B-16 melanomas grown subcutaneously on the flanks of male CBA mice, with a diameter of 8 mm were extracted and immersed in physiological saline before imaging. Tumors were then placed in a plastic holder, sealed with electrodes on both sides and inserted into the magnet with the axis perpendicular to the direction of the static magnetic field. The electrodes were connected to a DC voltage amplifier (0-300 V) that produced pulses with variable length, synchronized with the imaging sequence. To determine the influence of geometry of the electric field lines defined by electrodes on electric current density spatial distribution, two different shapes of electrodes were used—a plate and a needle. CDI images were obtained by using either two flat, two point electrodes or flat and point electrodes (Fig. 1b).

MRI and CDI Measurements

In vivo MRI was performed on 200 MHz Bruker Biospec system. *In vitro* MRI was performed on a 100 MHz Bruker

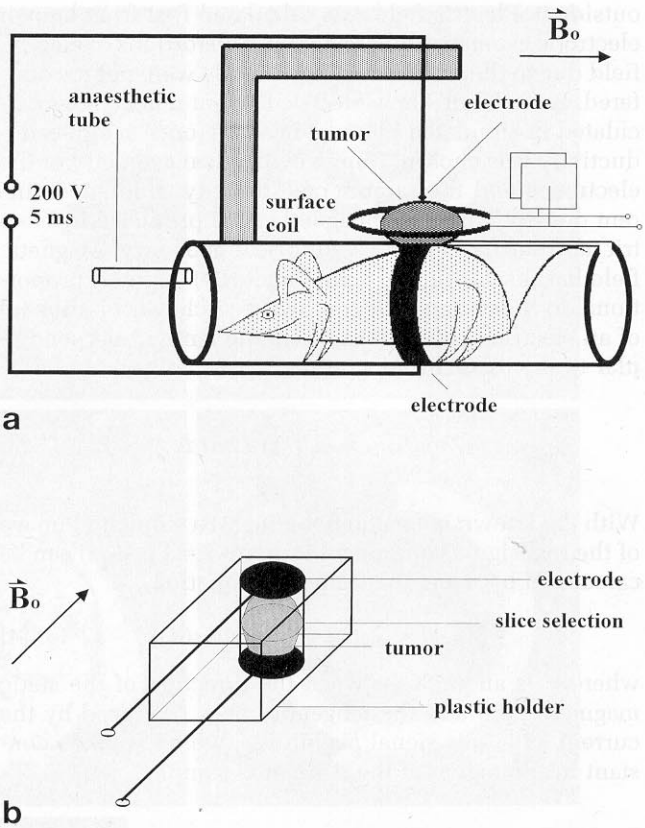

FIG. 1. Setup for the CDI of tumor (a) *in vivo,* (b) *in vitro.*

Biospec system equipped with microimaging gradient coils and a solenoid RF coil with a diameter of 20 mm. In both cases imaging conditions were: TR = 2500 ms, TE = 30 ms, FOV = 3 cm, slice thickness = 2 mm, MATRIX = 256 × 256, T_c = 5 ms and voltage applied U = 160 V. To reduce thermal tissue damage no signal averaging was used for *in vivo* measurements, while *in vitro* 10 scans were averaged so that imaging time was 17 min. Two current pulses (T_c) of total duration 5 ms and average current density 2500 A/m^2 were found to be the best compromise between sensitivity of CDI and tissue damage produced by the electric pulses. Current was controlled with an oscilloscope and average current density in central plane (Fig. 1) then computed from sample geometry. Conventional MRI of the central transverse slice was followed by MRI in the presence of electric current. To construct the map of electric current density spatial distribution (j_z), tumors in all *in vitro* experiments were imaged in two perpendicular orientations as required by theory. For *in vivo* experiments imaging was performed only in one sample orientation. CDI maps were calculated by computer simulation of CDI, which gave a similar real component of the signal as in the measured ones.

Numerical Simulations

Images of simulated real signal component on Figs. 3d and 3h and corresponding simulated current density images Figs. 3c and 3g were calculated assuming that MR signal is constant inside the simulated object and zero

outside it. Electric field was calculated first from known electrode geometry, where possible distortions of electric field due to the influence of the sample were not encountered. From Ohm's law, electric current density was calculated in simulated plane of imaging, once sample conductivity was chosen. Due to cylindrical geometry of the electrodes and the sample conductivity, simulated current density image and magnetic field produced by electric current have also a cylindrical geometry. Magnetic field has just tangential component (B_ϕ) which is proportional to the surface integral over a circle with radius (ρ) of an electric current density component (j_z) perpendicular to the plane of integration:

$$2\pi\rho B_\phi(\rho) = \mu_0 \int_0^\rho j_z(r) 2\pi r dr \qquad [3]$$

With the known magnetic field Eq. [3] a simulated image of the real signal component in point $\vec{r} = (\rho, \phi, z)$ can be calculated by using the following equation

$$S(\rho,\phi) = S_0 \sin(\gamma T_c B_\phi(\rho)\cos(\phi)) \qquad [4]$$

where ϕ is an angle between the direction of the static magnetic field and the tangential field produced by the current and S_0 is signal magnitude, which is taken constant in the region of the simulated sample.

RESULTS

Figures 2a and 2d show conventional *in vitro* magnitude MR images through a SA-1 sarcoma that was extracted from male mice before imaging. The necrotic center of both tumors had either no (Fig. 2a) or low (Fig. 2d) signal intensity with high signal intensity on the periphery. Maps of spatial electric current density distribution are shown in Figs. 2b and 2e. As required for CDI, tumors were imaged in two spatially perpendicular orientations and then maps of electric current density were calculated. Figures 2c and 2f show the measured real component of the signal for both tumors with dark and bright stripes that are attributed to the presence of electric currents. Only one of two measured spatially perpendicular orientations is shown.

Figures 3a and 3e show conventional *in vivo* magnitude MR images through T50/80 mammary carcinomas. The tumor in Fig. 3e is surrounded by dermal edema. Computer simulation of current density images, which gives similar real component of the signal (Figs. 3d, 3h) as the measured ones (Figs. 3c, 3g) are shown in Figs. 3b and 3f.

Figure 4a shows a conventional *in vitro* magnitude MR image through a B-16 melanoma. CDI images obtained with two types of electrodes are shown in Figs. 4b and 4c—both were flat in the case of Fig. 4b and one was flat and the other was a point electrode in the case of Fig. 4c.

DISCUSSION

Data show that CDI can generate maps of spatial distribution of electric currents through tumors. Specifically, maps of current density through T50/80 mammary carcinomas and SA-1 sarcomas show that current density can be higher in the tumor periphery (Figs. 3a and 3f) or distributed through the entire volume of the tumor (Figs. 2f and 3b).

Data also show that observation of the real component of the signal can sometimes simplify the imaging procedure as in Figs. 3a and 3e, where the electric current distribution was simulated on the basis of the agreement of the calculated real component of the signal (Figs. 3d and 3h) with the measured one (Figs. 3c and 3g).

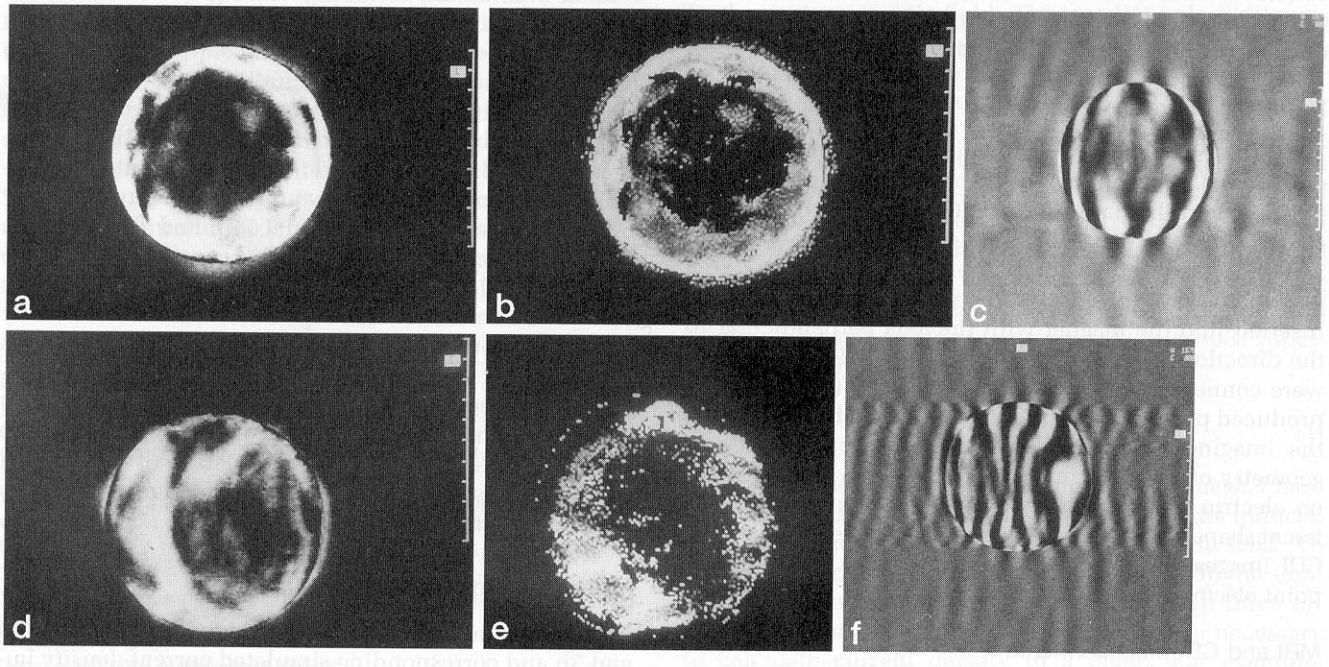

FIG. 2. *In vitro* CDI data from symmetric (upper raw) and nonsymmetric (lower raw) SA-1 sarcoma ((a) and (d) represent conventional MRI, (b) and (e) CDI from two orientations, (c) and (f) real component of the signal in *x* axis).

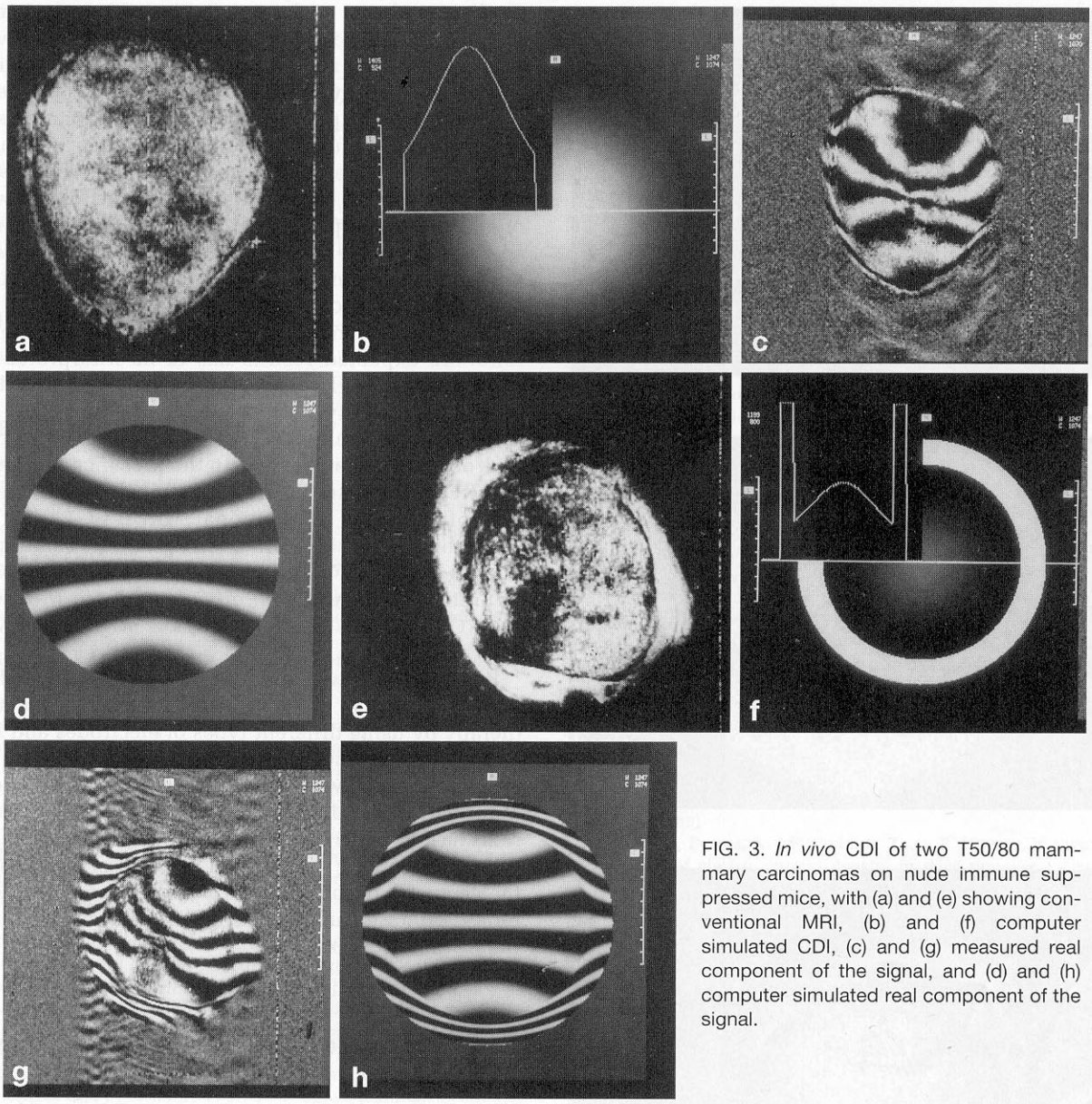

FIG. 3. *In vivo* CDI of two T50/80 mammary carcinomas on nude immune suppressed mice, with (a) and (e) showing conventional MRI, (b) and (f) computer simulated CDI, (c) and (g) measured real component of the signal, and (d) and (h) computer simulated real component of the signal.

CD images are a representation of spatial distribution of electric currents. According to Ohm's law:

$$j = \sigma E \quad [5]$$

conductivity (σ) through tumor can be obtained as well, if electric field (E) distribution is known. This is relatively straight forward in the case of two flat electrodes (Fig. 4b), where electric field has the same magnitude through the imaging plane, if one assumes that a material is only a small perturbation in the fields (31). Results of nonflat electrodes should not be misinterpreted as conductivity distribution images, even though in principal they can be calculated from known electrode geometry. The Appendix describes calculations of E for the electrode types we have used. Figure 4 shows experimental results in the case of melanomas where two flat electrodes produced current throughout the entire tumor (Fig. 4b), while one flat and an opposing point electrode produced stronger electric field in the central region of the tumor (Fig. 4c). These images can be predicted only if assuming homogeneous conductivity (see Appendix) and in addition, results are important because actual current distribution does not depend only on electrode geometry but, also on their tissue contact, which is hard to control (32).

A number of reports have described the use of electrochemotherapy to markedly increase the uptake of various drugs by the tumor cells and thereby increasing their cytotoxcicity. Yet a knowledge of CD spatial distribution was lacking. Literature data on CDI are limited to theoretical considerations but few illustrations of biological applications show that sufficient sensitivity can be achieved (25-29). The value of results presented in this paper is in the direct comparison with electrochemotherapy data since currents of the same magnitude as those used in electrochemotherapy were applied (16-22).

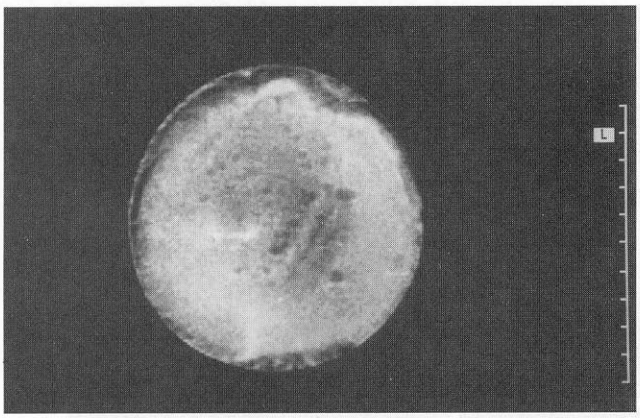

a

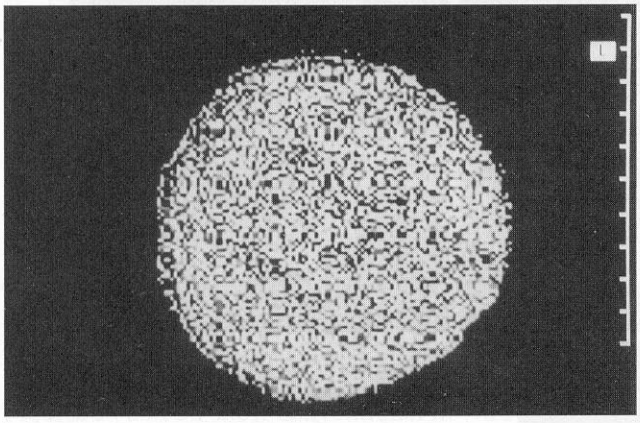

b

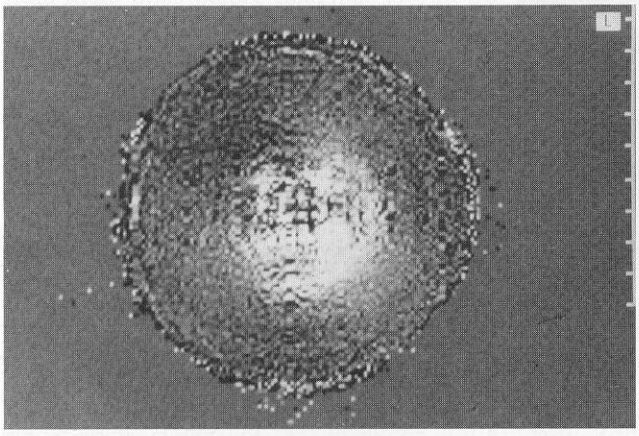

c

FIG. 4. Comparison of CDI data from B-16 melanoma using flat-flat (b) and point-flat (c) electrodes ((a) represents conventional MRI, (b) CDI using flat-flat electrodes, and (c) CDI using point-flat electrodes).

Since CDI enables one to directly follow electric current distribution, different electrode geometry was used. The method can be applied to prove the hypothesis that the effect of electrochemotherapy strongly depends on the placing and geometry of the electrodes.

The main limitation of the method is the requirement for imaging in two spatially perpendicular orientations, which may consequently limit the application of CDI to small animals, or to the extremities of large animals or human subjects in conventional magnets. However, open-architecture magnets and dedicated orthopedic imaging systems may allow the use of this technique. Tumors are an example when this limitation can be sometimes overcome due to predictable CD distribution (Fig. 3), yet at the expense of accuracy. In addition, just one component of CD distribution (j_z) obtained from two (or one) spatially perpendicular orientations of the sample, corresponds to whole current only in the case where nonparallel current contributions can be neglected as for two plane electrodes or in a highly elongated electrode geometry. In the situation where nonparallel currents are expected results has to be interpreted with caution, especially when discussing the correlation with ECT. Finally, the presence of conducting electrodes within the imaging system may cause artifacts and/or pose a safety hazard in the presence of magnetic and RF fields. The limiting factor in CDI can also be a lack of signal in conventional MRI (Fig. 2a). In such cases the lack of signal in CD image on the same spot in necrotic center (Fig. 2b) cannot be unambiguously interpreted. The low signal on conventional MRI with a high CD would show on CDI as a bright spot with a high noise level.

Future studies will focus on the combined use of ECT, MRI, and CDI in following the time course of tumor therapy by using different types of electrodes and in the study of other tissues.

In conclusion, we have used CDI to map electric current distribution through tumors. The magnitude of currents has the same magnitude as in ECT. Various patterns of current density distribution were observed. Changing the geometry of the electrodes has changed electric current distribution and limited electric current effect in the tumor to its center.

APPENDIX: EFFECT OF ELECTRODE GEOMETRY ON ELECTRIC FIELD DISTRIBUTION

Various types of electrodes produce different electrical fields $\vec{E}$ that differ in their spatial distribution. From Ohm's law, $\vec{j} = \sigma \vec{E}$ follows as a consequence that electric current density $\vec{j}$ is proportional to electric field $\vec{E}$ produced by the electrodes. Three different electrode types were taken under theoretical consideration: flat electrodes, point electrodes, and a pair of point and flat electrodes. In all three cases a cylindrical symmetry is preserved—electric current density has a cylindrical symmetry. Electric field in the central plane between the electrodes was calculated by taking into account the electrode geometry (33):

flat-flat electrodes:

$$E = E_0 \qquad [6]$$

point-point electrodes:

$$E = E_0 \frac{1}{(1 + (\frac{2\rho}{a})^2)^{3/2}} \qquad [7]$$

flat-point electrodes:

$$E = \frac{E_0}{8}\left(\frac{9}{\left(1+\left(\frac{2\rho}{a}\right)^2\right)^{3/2}} - \frac{1}{\left(1+\left(\frac{2\rho}{3a}\right)^2\right)^{3/2}}\right) \quad [8]$$

In the Eqs. [6-8] a indicates the shortest distance between the electrodes, 114 the radius in cylindrical symmetry and E_0 electric field in the middle of the plane.

ACKNOWLEDGMENTS

The authors thank Gregor Seröa and Maja Čemažar for useful discussions and help with tumor work.

REFERENCES

1. B. W. Watson, The treatment of tumours with direct electric current. *Med. Sci. Res.* **19,** 103–105 (1991).
2. S. L. David, D. R. Absolom, C. R. Smith, J. Gams, M. A. Herbert, Effect of low level direct current on *in vivo* tumor growth in hamsters. *Cancer Res.* **45,** 5626–5631 (1985).
3. L. Samuelsson, L. Jonsson, I. L. Lamm, C. J. Linden, S. B. Ewers, Electrolysis with different electrode materials and combined with irradiation for treatment of experimental rat tumors. *Acta Radiol.* **32,** 178–181 (1990).
4. E. Heiberg, W. J. Nalesnik, C. Janney, Effects of varying potential and electrolytic dosage in direct current treatment of tumors. *Acta Radiol.* **32,** 174–177 (1991).
5. D. Miklavčič, G. Serša, L.Vodovnik, S. Novakovič, F. Bobanovič, R. Golouh, S. Reberöak, Local treatment of murine tumors by electric direct current. *Electro. Magnetobiol.* **11,** 109–125 (1992).
6. A. A. Marino, D. Morris, T. Arnold, Electrical treatment of Lewis lung carcinoma in mice. *J. Surg. Res.* **41,** 198–201 (1986).
7. D. M. Morris, A. A. Marino, Percutaneous electrical treatment of tumors, *in* "Proc., AACR, 79th Annual Meeting, New Orleans, 1988," p. 219.
8. C. E. Humprey, E. H. Seal, Biophysical approach towards tumour regression in mice. *Science* **130,** 388–390 (1959).
9. D. Miklavčič, G. Serša, M. Kryzanowski, S. Novakovič, F. Bobanovič, R. Golouh, L. Vodovnik, Tumour treatment by direct electric current tumor temperature and pH, electrode material and configuration. *Bioelectrochem. Bioenerg.* **30,** 209–220 (1993).
10. D. Miklavčič, G. Serša, S. Magister, S. Reberöek, L. Vodovnik, Low intensity direct current as an antitumour agent? *Radiol. Iugosl.* **24,** 75–78 (1990).
11. B. Rosenberg, L. Van Camp, T. Krigas, Inhibition of cell division in Escherichia Coli by electrolysis products from a platinum electrode. *Nature* **205,** 698–699 (1965).
12. B. T. Mortenson, J. Bojsen, Evidence for growth inhibition by platinum electrodes at low current level. *J. Biomed. Eng.* **4,** 103–106 (1982).
13. D. Miklavčič, A. Fajgelj, G. Seröa, Tumour treatment by direct electric current - electrode material deposition. *Bioelectrochem. Bioenerg.* **35,** 93–97 (1994).
14. N. J. F. Dodd, J. V. Moore, T. V. Taylor, S. Zhao, Preliminary evaluation of low-level direct current therapy using magnetic resonance imaging and spectroscopy. *Phys. Med.* **9,** 285–289 (1993).
15. M. Yokoyama, T. Itaoka, H. Nakajima, T. Ikeda, T. Ishikura, S. Nitta, The use of direct current for local destruction of cancer tissue. *Jpn. J. Cancer Chemother.* **16,** 1412–1417 (1989).
16. L. Samuelson, L. Jonsson, Electrolytic destruction of lung tissue: electrochemical aspects. *Acta Radiol. Diagn.* **21,** 711–714 (1980).
17. L. C. Benov, P. A. Antonov, S. R. Ribarov, Oxidative damage of the membrane lipids after electroporation. *Gen. Physiol. Biophys.* **13,** 85–97 (1994).
18. L. M. Mir, S. Orlowski, J. Belehradek Jr, J. Tessie, M. P. Rols, G. Seröa, D. Miklavčič, R. Gilbert, R. Heller, Biomedical applications of electric pulses with special emphasis on antitumour electrochemotherapy. *Bioelectrochem. Bioenerg.* **38,** 203-207 (1995).
19. G. Serša, M. Čemažar, D. Miklavčič, Antitumour effectiveness of electrochemotherapy with cis-diamminedichloroplatinum(II) in mice. *Cancer Res.* **55,** 3450–3455 (1995).
20. R. Heller, Treatment of cutaneous nodules using electrochemotherapy. *J. Florida Med. Assoc.* **82,** 147–150 (1995.
21. L. M. Mir, M. Belehradek, C. Domenge, S. Orlowski, B. Poddevin, J. Belehradek Jr., G. Schwab, B. Luboinski, C. Paoletti, Electrochemotherapy, a new antitumor treatment: first clinical trial. *C. R. Acad. Sci. Paris Serie III,* **313,** 613–618 (1991).
22. M. Belehradek, C. Domenge, B. Luboinski, S. Orlowski, J. Belehradek Jr., L. M. Mir, Electrochemotherapy, a new antitumor treatment. First clinical phase I-II trial. *Cancer* **72,** 36940–700 (1993).
23. L. M. Mir, C. Roth, S. Orlowski, F. Quintin-Colonna, D. Fradelizi, J. Belehradek Jr., P. Kourilsky, Systemic antitumour effects of electrochemotherapy combined with histocompatible cells secreting interleukin-2. *J. Immunother.* **17,** 30–38 (1995).
24. G.C. Scott, M.L.G. Joy, R.L. Armstrong, R.M. Henkelman, Sensitivity of magnetic resonance current-density imaging. *J. Magn. Reson.* 97, 235–254 (1992).
25. I. Serša, O. Jarh, F. Demsar, Magnetic resonance microscopy of electric currents. *J. Magn. Reson.* **111A,** 93–99 (1994).
26. M. Joy, G. Scott, M. Henkelman, In vivo detection of applied electric currents by magnetic resonance imaging. *Magn. Reson. Imaging* **7,** 89–94 (1989).
27. I. Serša, K. Beravs, N. J F. Dodd, S. Zhao, F. Demsar, In vivo determination of electric current density in mice tumours - a new approach for monitoring the efficiency of electrochemo tumour therapy, *in* "Proc., SMR/ESMRMB, 3rd and 11th Annual Meeting, Nice, 1995," p. 689.
28. M. G. L. Joy, V. P. Lebedev, J. Gatti, Current density in sections through rabbit brain, *in* "Proc., SMRM, 11th Annual Meeting, Berlin, 1992," p. 1404.
29. S. Zhao, N. J. F. Dodd, J. M. Hawnaur, I. Isherwood, In vivo imaging of electrical current density distribution in mouse tumour, *in* "Proc., SMRM, 12th Annual Meeting, New York, 1993," p. 1368.
30. G. Serša, M. Čemažar, D. Semrov, D. Miklavčič, Changing electrode orientation improves the efficacy of electrochemotherapy of solid tumours in mice. *Bioelectrochem. Bioenerg.* **39,** 61–66 (1996).
31. H. P. Schwan, Electrode polarization impedance and measurements in biological materials. *Annals N.Y.Acad.Sci.* **148,** 191–209 (1968).
32. K. R. Foster, Dielectric properties of tissues, *in* "The Biomedical Engineering Handbook" (J. D. Bronzino, Ed.), pp. 1385–1394, CRC Press, Boca Raton, FL, 1995.
33. W. R. Smythe, "Static and Dynamic Electricity," McGraw-Hill, New York, 1968.